

The Effect of Temperature on the Adsorption Behavior and Inhibition Performance of a Pyrimidine-Type Inhibitor at Medium Temperature Range (25°C to 80°C)

Yi He, Shuai Ren, Xi Wang, David Young, Marc Singer
Institute for Corrosion and Multiphase Technology
Department of Chemical and Biomolecular Engineering
Ohio University
342 West State Street
Athens, OH 45701, USA

Maalek Mohamed-Saïd
TotalEnergies
OneTech - CSTJF, Avenue Larribau
F-64018 Pau
France

Sheyla Camperos
TotalEnergies
OneTech - TRTG - TotalEnergies Research &
Technology Gonfreville
BP 27 76 700 Harfleur – FRANCE

ABSTRACT

In the oil and gas industry, long-distance transmission of produced hydrocarbons is usually carried out in large-diameter steel pipelines. However, water co-produced with the oil and gas, combined with CO₂ or H₂S, can cause severe corrosion of internal pipeline surfaces. A widely applied, economically effective method of corrosion control is to inject corrosion inhibitors (CIs). Adsorption of the organic molecules on surfaces through heteroatom functionalities, containing nitrogen, oxygen, sulfur and/or phosphorus, can markedly change the corrosion resistance characteristics of the exposed metal, typically mild steel for pipelines. Among these organic compounds, heterocyclic molecules containing nitrogen atoms have been demonstrated to be excellent corrosion inhibitors (CIs) for many alloys in various aggressive media. In this research, surface saturation concentrations, as well as inhibition efficiencies of tetradecyltetrahydropyrimidinium (THP-C14), were determined at 25, 55 and 80°C by monitoring linear

polarization resistance (LPR) until the corrosion of the steel specimens stabilized. Potentiodynamic sweeps were obtained at the end of each test. The five most frequently used adsorption isotherms, which correlate coverage and inhibitor concentration using different assumptions, were reviewed and adapted to fit the corrosion inhibition behavior. These isotherms were evaluated based on their goodness of fit and the relevance of their underlying assumptions. In addition, the equilibrium constants of adsorption/desorption (K_{AD}) at 25, 55 and 80°C were determined by fitting the steady state experimental data. Finally, the changes of activation energy with and without inhibitor at 25, 55 and 80°C were calculated and compared.

Keywords: corrosion inhibitors, inhibition efficiency, surface saturation concentration, adsorption isotherms, changes of activation energy

INTRODUCTION

In the oil and gas industry, long-distance transportation of petroleum and related products is usually carried out in large-diameter carbon steel pipelines. Water present with the oil, along with corrosive species such as CO_2 , H_2S and organic acids, causes severe corrosion of the inner pipe walls.¹ An effective method of controlling corrosion is to continuously inject corrosion inhibitors into pipelines conveying oil-water mixtures. As corrosion occurs on water wetted metal surfaces, corrosion inhibitor (CI) molecules form protective films which retard electrochemical reaction rates at the water-metal interface,² thereby protecting carbon steel pipes against CO_2 ("sweet") corrosion and H_2S ("sour") corrosion. Most commercial CIs are a complex mixture of several compounds that contain surfactant-type active ingredients, such as imidazoline, amine, phosphate ester, and quaternary ammonium derivatives.³ Adsorption of organic molecules on surfaces through heteroatom functionalities, containing nitrogen, oxygen, sulfur and/or phosphorus, can markedly change the corrosion resistance properties of metals. Among these organic compounds, heterocyclic molecules containing nitrogen atoms have been demonstrated to be excellent corrosion inhibitors (CIs) for many metals and alloys in various aggressive media.⁴⁻⁶ The performance of quaternary ammonium-type, imidazolium-type and thiol-type corrosion inhibitor model compounds is the focus of intense study⁷⁻¹⁰ in order to deliver descriptive and predictive inhibition models, as well as inhibitor testing methodologies, for industrial users of these compounds.

The goal of the current research is to develop an inhibitor testing protocol and to develop an accurate inhibition prediction tool. Experiments that cover a range of experimental conditions, including inhibitor concentrations and temperatures, are being undertaken. These will enable the determination of fundamental corrosion inhibition parameters as the inputs for an electrochemical model aimed at facilitating the prediction of inhibitor performance, at any given CI concentration and for a broad range of experimental conditions. This research also investigated the use of different adsorption isotherms to correlate coverage and inhibitor concentration at different temperatures.

Corrosion Inhibition at Elevated Temperatures

The available literature on the effect of temperature on inhibition efficiency can appear contradictory. Ding, *et al.*¹¹ performed a series of experiments in a standard 2L glass cell at low to medium temperature (25°C, 50°C and 80°C) to characterize adsorption kinetics, using imidazoline-type and quat-type inhibitors. These experiments included general corrosion inhibition tests using linear polarization resistance (LPR) measurements and direct determination of adsorption behavior using a quartz crystal

microbalance (QCM). Both test methods yielded similar trends for the two inhibitors tested. This suggested that the loss of inhibition efficiency as temperature increased was a result of desorption being favored at higher temperatures. However, Bentiss, *et al.*¹² studied the role of a thiazazole-type inhibitor on the corrosion behavior of mild steel in an acidic environment at different temperatures (30°C-60°C). They found that the efficiency of the inhibitor increased with temperature and attributed the temperature dependency as a sign of chemical adsorption; indicating that the chemical adsorption is more favorable than physical adsorption at the higher temperature. However, there was no further discussion on what correlates the temperature dependent behavior with the nature of chemisorption. Zhang, *et al.*^{13, 14} examined the inhibition performance of three different halogen-substituted imidazoline derivatives (labeled as 1-IM, 2-IM, 3-IM) for mild steel in a hydrochloric acid solution from 30°C to 70°C. They noticed that the performance of the two inhibitors either decreased (1-IM, 3-IM) or only slightly changed (2-IM) at elevated temperatures. The authors concluded that these three inhibitors are mainly physisorbed on metal surfaces. The dominance of chemisorption or physisorption depends upon the chemistry (brine, Cl molecules and metallic surface charge), it is not only temperature dependent.

Understanding the role of high temperature on inhibition performance is a complex task. The understanding of the corrosion inhibition mechanism at low temperatures serves as a solid foundation for research at higher temperatures. However, the role of temperature on corrosion inhibition is complex and differs from inhibitor to inhibitor. In addition, the understanding of the effect of temperature on inhibitor adsorption behavior is also limited. Therefore, the work in this paper is limited to adsorption, *i.e.*, excluding thermal degradation effects (if any).

Fitting of Different Adsorption Isotherms

In consideration of the several adsorption isotherms that are available, a proper model should be chosen to describe the adsorption and desorption process of THP-C14 molecules on the steel surface in the studied conditions. In this section, five adsorption isotherm models will be evaluated by fitting the steady state experimental data (C_{inh} vs. θ_{eq}). From the coefficient of determination (R^2) of fitting, the relative adequacy of these models to studied adsorption processes can then be discussed.

Before discussing the fitting results, the five utilized adsorption isotherm models are introduced, *i.e.*, the Langmuir, Temkin, Frumkin and Flory-Huggins/Dhar-Flory-Huggins models.

- (a) Langmuir model: Homogeneous surface, monolayer, and no interaction between adsorbed inhibitor molecules. When the adsorption-desorption process of the corrosion inhibitor has reached a point where the coverage remains unchanged with respect to time:¹⁵

$$C_{inh}K_{AD} = \left(\frac{\theta_{eq}}{1 - \theta_{eq}} \right) \quad (1)$$

Where θ_{eq} is the steady state surface coverage values at precise Cl concentrations. K_{AD} is the equilibrium constant of adsorption/desorption, which is equal to the ratio of the adsorption and desorption constants. C_{inh} is the bulk concentration of the Cl.

- (b) Temkin model: Heterogeneous surface, no molecular interactions, considering the surface is made up of a great number of small patches, on each of which the Langmuir isotherm is applicable.¹⁶

$$\theta_{eq} = \frac{1}{g} \ln (K_{AD} C_{inh}) \quad (2)$$

Where g is the adsorbent-adsorbate interaction constant.

- (c) Frumkin model: Heterogeneous surface, considering lateral interactions between adsorbed surfactant molecules.¹⁶

$$K_{AD} C_{inh} = \frac{\theta_{eq}}{1 - \theta_{eq}} \exp(-f\theta_{eq}) \quad (3)$$

Where f is a constant relating to the interactions between adsorbate molecules and is independent of θ . The Langmuir model is a specific case of Frumkin model with $f=0$.

- (d) Flory-Huggins/Dhar-Flory-Huggins model: Considers the substitution of adsorbed solvent by adsorbing molecules.¹⁶ Different from the Flory-Huggins model, the Dhar-Flory-Huggins isotherm has one exponential factor. Strictly, it is incorrect to refer to an isotherm containing the configurational term $\frac{\theta_{eq}}{\delta(1-\theta_{eq})^\delta}$, which is related to the arrangement of atom/molecules on the metal surface, as the “Flory-Huggins isotherm”, since Flory-Huggins statistics leads to an isotherm having a different form for the configurational term, which is $\exp(\delta - 1)$.

$$\text{Flory-Huggins:} \quad K_{AD} C_{inh} = \frac{\theta_{eq}}{\delta(1-\theta_{eq})^\delta} \quad (4)$$

$$\text{Dhar-Flory-Huggins:} \quad K_{AD} C_{inh} = \frac{\theta_{eq}}{e^{(\delta-1)}(1-\theta_{eq})^\delta} \quad (5)$$

Where δ is the number of solvent molecules substituted by an adsorbate molecule. The Langmuir model is a specific case of Flory-Huggins/Dhar-Flory-Huggins model with $\delta=1$.

By fitting the experimental data with these non-linear equations, the constants in these equations were determined and the fitting curves were plotted together with experimental data for comparison.

Changes of Activation Energy

Dominguez, *et al.*^{9,17}, have discussed the physical interpretation of the chemical component of the total activation energy in the electrochemical dissolution of steel. The effect of the alkyl tail length on the kinetics of the electrochemical process behind CO₂ corrosion of a UNS K03014 steel at pH 4.0 was investigated. The activation energy associated with the corrosion process was determined *via* an Arrhenius plot from charge transfer resistance measurements at the potential of zero charge (PZC). It was assumed that the rate constant of the iron dissolution was governed by the chemical component of the activation energy. This method^{9,17} used to obtain the difference in activation energy between uninhibited and maximum inhibited conditions, could be simplified since what the inhibition model needs are the activation energy differences between inhibited and uninhibited environments, which does not have to be evaluated at the PZC. Consequently, a new method has been proposed to obtain the activation energy change directly from the potential polarization curve. At a fixed potential, the difference in chemical activation energy can still be determined by the difference in total activation energy. In this paper, surface saturation concentration (C_{inh}) will be obtained by monitoring changes of corrosion rate with time in the electrolyte with different inhibitor concentrations.

The current densities in uninhibited (i_{un}) and maximum inhibited conditions ($i_{inh, max}$) can be represented by the following equations, considering the anodic current:

$$i_{un} = A \exp\left(-\frac{\Delta G_{un}^{\#}}{RT}\right) \exp\left(\frac{\alpha n F \eta}{RT}\right) \quad (6)$$

$$i_{inh, max} = A \exp\left(-\frac{\Delta G_{inh, max}^{\#}}{RT}\right) \exp\left(\frac{\alpha n F \eta}{RT}\right) \quad (7)$$

Where $A = n F C_R^s \frac{k_B T}{h}$, n is number of electrons transferred per mole; C_R^s is the concentration of a reactant at the metal-solution interface; k_B is the Boltzmann constant; h is the Planck constant; $\Delta G_{un}^{\#}$ is the activation energy without inhibitor at reversible potential (E_{rev}), and $\Delta G_{inh, max}^{\#}$ is the activation energy in maximum inhibited condition; and η is overpotential, the difference between applied potential and reversible potential ($E - E_{rev}$). F is the Faraday constant. R is the ideal gas constant, and T is the absolute temperature in Kelvin (K).

Considering the ratio of these two current densities:

$$i_{un}/i_{inh, max} = \exp\left(-\frac{\Delta G_{un}^{\#}}{RT}\right) / \exp\left(-\frac{\Delta G_{inh, max}^{\#}}{RT}\right) \quad (8)$$

Applying the natural logarithm on both sides of the above equation and rearranging yields:

$$\Delta G_{inh, max}^{\#} - \Delta G_{un}^{\#} = RT \ln (i_{un}/i_{inh, max}) \quad (9)$$

The above equation indicates that the activation energy difference between uninhibited and maximum inhibited conditions ($\Delta G_{inh, max}^{\#} - \Delta G_{un}^{\#}$) can be determined by the ratio of their corresponding current densities ($i_{un}/i_{inh, max}$), as long as the process is charge transfer controlled.

This paper is specifically related to the characterization of a model compound possessing a pyrimidine structural moiety (tetradecyl-1,4,5,6-tetrahydropyrimidinium, or THP-C14), which is found in particular commercial CI formulations; its synthesis and characterization as a model compound is reported elsewhere.¹⁸ The scope of work not only involves the corrosion inhibition performance of selected corrosion inhibitor but also the investigation of adsorption behavior. In this research, surface saturation concentrations as well as inhibition efficiencies at 25, 55 and 80°C were determined by monitoring linear polarization resistance (LPR) until the corrosion of the steel specimens stabilized. Potentiodynamic sweeps were obtained at the end of each test. The five most frequently used adsorption isotherms, which correlate coverage and inhibitor concentration using different assumptions, are reviewed and adapted to fit the corrosion inhibition behavior of tetradecyltetrahydropyrimidinium (THP-C14). These isotherms were evaluated based on their goodness of fit and the relevance of their underlying assumptions. In addition, the equilibrium constants of adsorption/desorption (K_{AD}) at 25, 55 and 80°C were determined by fitting the steady state experimental data. Finally, the changes of activation energy with and without inhibitor at 25, 55 and 80°C were calculated and compared.

EXPERIMENTAL METHODOLOGY

Materials and Chemicals

UNS G10180¹ carbon steel (C1018) specimens with a ferritic-pearlitic microstructure have been used for the electrochemical measurements. The 5 wt.% NaCl electrolyte was prepared by dissolving sodium chloride (NaCl) in deionized water and then saturated with CO₂ at 25, 55 and 80°C and 1 bar total pressure to facilitate deoxygenation.

The CI model compound employed in this work, *i.e.*, tetradecyltetrahydropyrimidinium (THP-C14), was synthesized in-house as described in a prior paper.¹⁸ The product THP-C14 is of *ca.* 99%+ purity, as determined by ¹H-NMR, with a near 100% yield.

Electrochemical Measurements

A three-electrode setup (Figure 1.) was used to perform electrochemical experiments, with a C1018 rotating cylinder electrode (RCE) as a working electrode, a platinum-coated titanium mesh counter electrode, and an Ag/AgCl (KCl saturated) reference electrode. Before each experiment, the RCE was sequentially polished with 240, 400 and 600 grit silicon carbide abrasive papers, cleaned with isopropanol in an ultrasonic bath, and air-dried. The solution was deoxygenated for 2 hours by sparging with CO₂ before the introduction of the working electrode. After the RCE was inserted into the glass cell, a 20-minute pre-corrosion test was conducted (Figure 1.) to determine whether the initial corrosion rate (CR) was close to the blank test and to ensure no contamination from the previous test. To minimize the noise in electrochemical measurements caused by CO₂ sparging, the sparge tube was retracted into the headspace during data acquisition. The solution was purged with CO₂ throughout the test to prevent air ingress and to saturate the test solution with CO₂. The pH was adjusted by adding deoxygenated hydrochloric acid or sodium bicarbonate solution during each experiment.

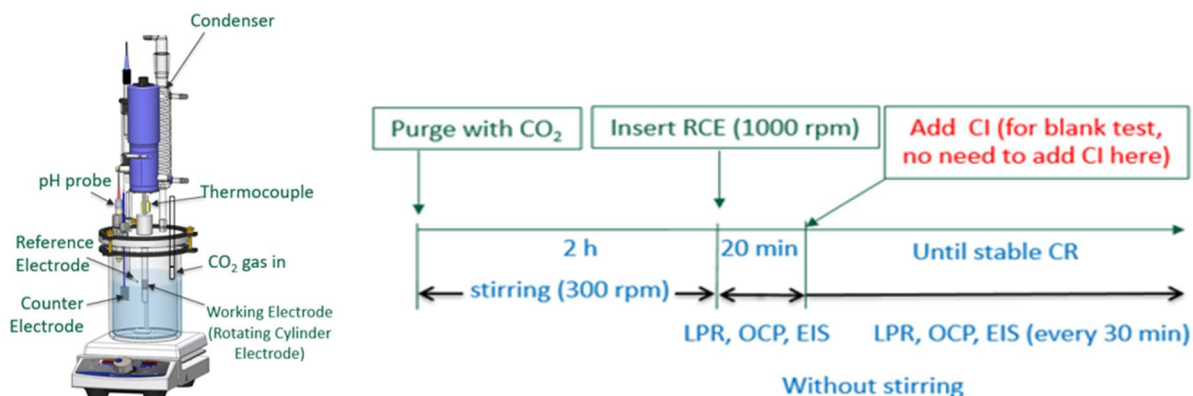


Figure 1. Three-electrode setup and procedure used for corrosion experiments².

The corrosion rate was assessed by measuring linear polarization resistance (LPR) with a scan range from -5 mV to +5 mV *versus* OCP, a scan rate of 0.125 mV/s and a B value of 26 mV. The B value for these experiments was taken from previous research conducted on mild steel in a CO₂ environment¹⁹ and was used in the analysis of all the experimental data reported herein. The cathodic sweep was obtained by polarizing from OCP to approximately -0.7 V *versus* OCP. The anodic potentiodynamic polarization was performed in the positive direction to +0.3 V *versus* OCP. Corrosion inhibitors were

¹ UNS numbers are listed in *Metals and Alloys in the Unified Numbering System*, published by the Society of Automotive Engineers (SAE International) and cosponsored by ASTM International.

² Image courtesy of Cody Shafer, ICMT, Ohio University.

© 2022 Association for Materials Protection and Performance (AMPP). All rights reserved. No part of this publication may be reproduced, stored in a retrieval system, or transmitted, in any form or by any means (electronic, mechanical, photocopying, recording, or otherwise) without the prior written permission of AMPP.

Positions and opinions advanced in this work are those of the author(s) and not necessarily those of AMPP. Responsibility for the content of the work lies solely with the author(s).

tested at different concentrations. Each experiment was performed three times. The electrochemical measurements were conducted with a Gamry Reference 600. Table 1 shows the test matrix for the experimental conditions.

Table 1. Experimental matrix for electrochemical experiments

Description	Parameters
Working electrolyte	5 wt.% NaCl
Material	Carbon steel UNS G10180 (C1018)
Sparge gas	CO ₂
Temperature	25, 55 and 80°C
pH	4.5
Cl model compound	1-tetradecyl-1,4,5,6-tetrahydropyrimidinium bromide (THP-C14)
RCE velocity	1000 rpm
Measurement methods	LPR, EIS, potentiodynamic sweeps

RESULTS AND DISCUSSION

Temperature Effect on Surface Saturation Concentration

The surface saturation concentration is the minimum concentration that yields the maximum efficiency of a corrosion inhibitor. As proposed by Hackerman, *et al.*, corrosion inhibitors will continue to adsorb on the metal surface until the surface is saturated with the inhibitor;²⁰ any further addition of the inhibitor to the bulk solution does not result in a further decrease in the corrosion rate. The amount of the inhibitor added is called the surface saturation concentration.²⁰

Figure 2 shows the corrosion rate measurements of uninhibited and inhibited C1018 by THP-C14 for different concentrations at different temperatures. The C1018 RCE was immersed in 5 wt.% NaCl solution at 25, 55 and 80 °C. Solution pH was adjusted to 4.5 ± 0.5 before each test. At 25°C (Figure 2 (a)), in the absence of inhibitor, the corrosion rate was 2.01 ± 0.13 mm/yr. In the presence of THP-C14, the corrosion rate gradually decreased with increasing inhibitor concentration from 0.25 to 4 ppm_w. When the Cl concentration is above 4 ppm_w, the corrosion rate remained low at 0.11 ± 0.02 mm/yr and relatively insensitive to the inhibitor concentration. The surface saturation concentration of THP-C14 in 5 wt.% NaCl was determined to be within the range of 1 to 4 ppm_w. Using the same method to analyze the data in Figure 2 (b) and (c), the surface saturation concentration of THP-C14 at 55 and 80°C was determined to be within the range of 50 to 70 ppm_w and 800 to 1600 ppm_w, respectively. The results showed that surface saturation concentration increased with increasing temperature. However, the range of surface saturation concentration at 80°C is unusual for an actual pipeline mitigation strategy, even at $T > 80^\circ\text{C}$; the aim of the current work is not to design a performant inhibitor at high temperature but to understand the inhibition mechanism at high temperature. This report will continue the investigation even if the dosage is abnormally high. At 80°C (Figure 2 (c)), for concentrations from 17.5 to 800 ppm_w, the corrosion rates displayed an incubation time associated with the onset of inhibitor effectiveness. It is noteworthy that for the inhibitor concentration of 1600 ppm_w, there is no incubation time. At higher temperatures, the adsorption and desorption constants will increase, increasing the rate of both adsorption and desorption processes.²¹⁻²³ The experimental results suggest that, in this case, the desorption rate increases more

than the adsorption rate, while the adsorption process is still dominant. Consequently, it is likely to take more time to form a protective inhibitor layer on the surface. With a higher concentration of corrosion inhibitors, the inhibitor molecules are more available, so the onset of inhibition is shorter.

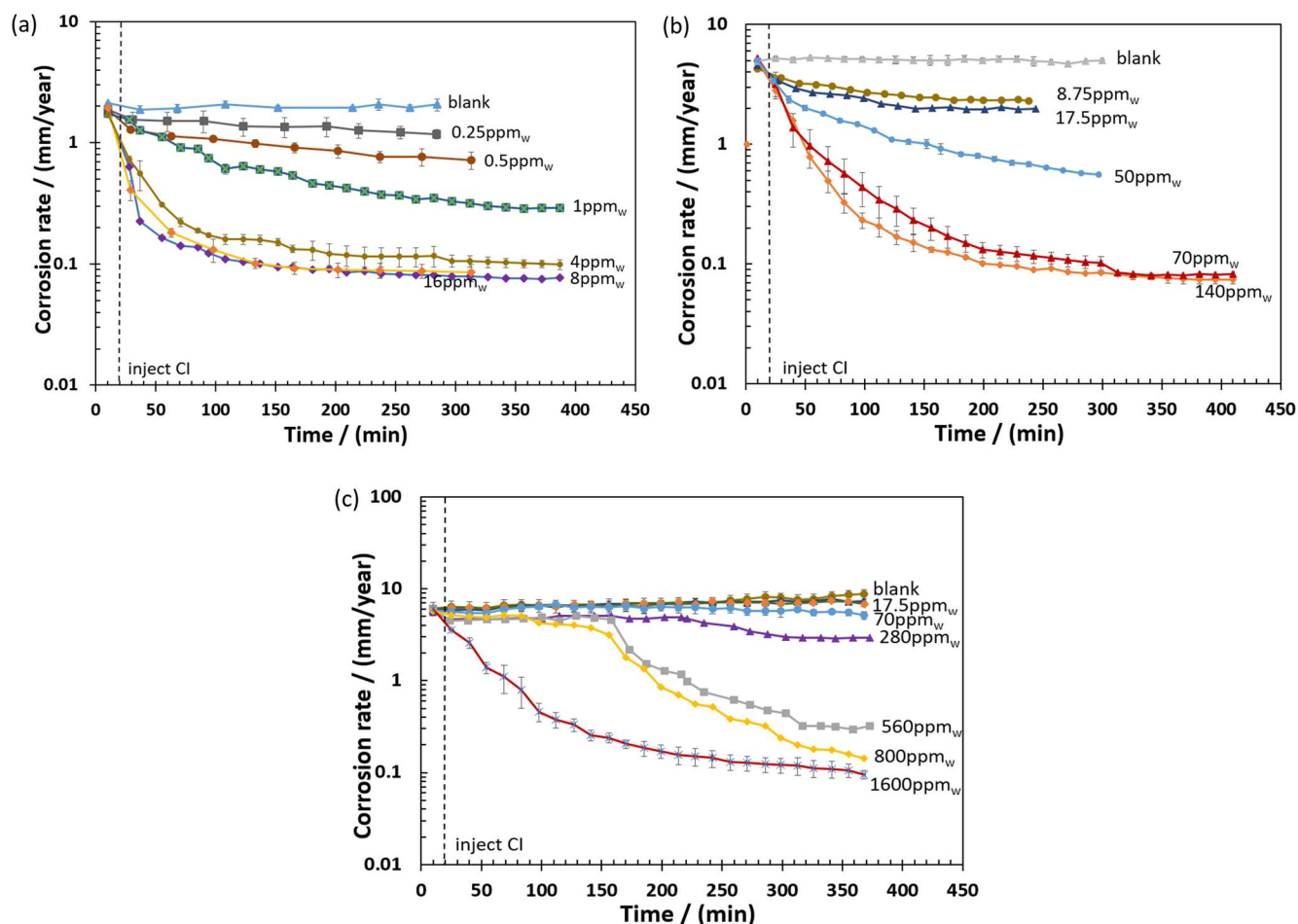


Figure 2. The corrosion rate of the C1018 carbon steel in the presence and absence of THP-C14 at (a) 25°C (b) 55°C and (c) 80°C as a function of time.

Figure 3 shows sets of potentiodynamic polarization curves for the CO₂ corrosion of C1018 carbon steel at different THP-C14 corrosion inhibitor concentrations at 25, 55 and 80°C. Compared with the blank test, the addition of different concentrations of corrosion inhibitor seemed to retard both the anodic and cathodic reactions. The same phenomenon was also observed with BDA-C14 (benzyltrimethyltetradecylammonium), as the charge transfer regions were more retarded while the limiting current remained unaffected.^{9,17} According to Dominguez, *et al.*, this effect for BDA-C14 was due to the adsorption of organic corrosion inhibitors: only charge transfer reactions are retarded while limiting currents remain unaffected.^{9,17}

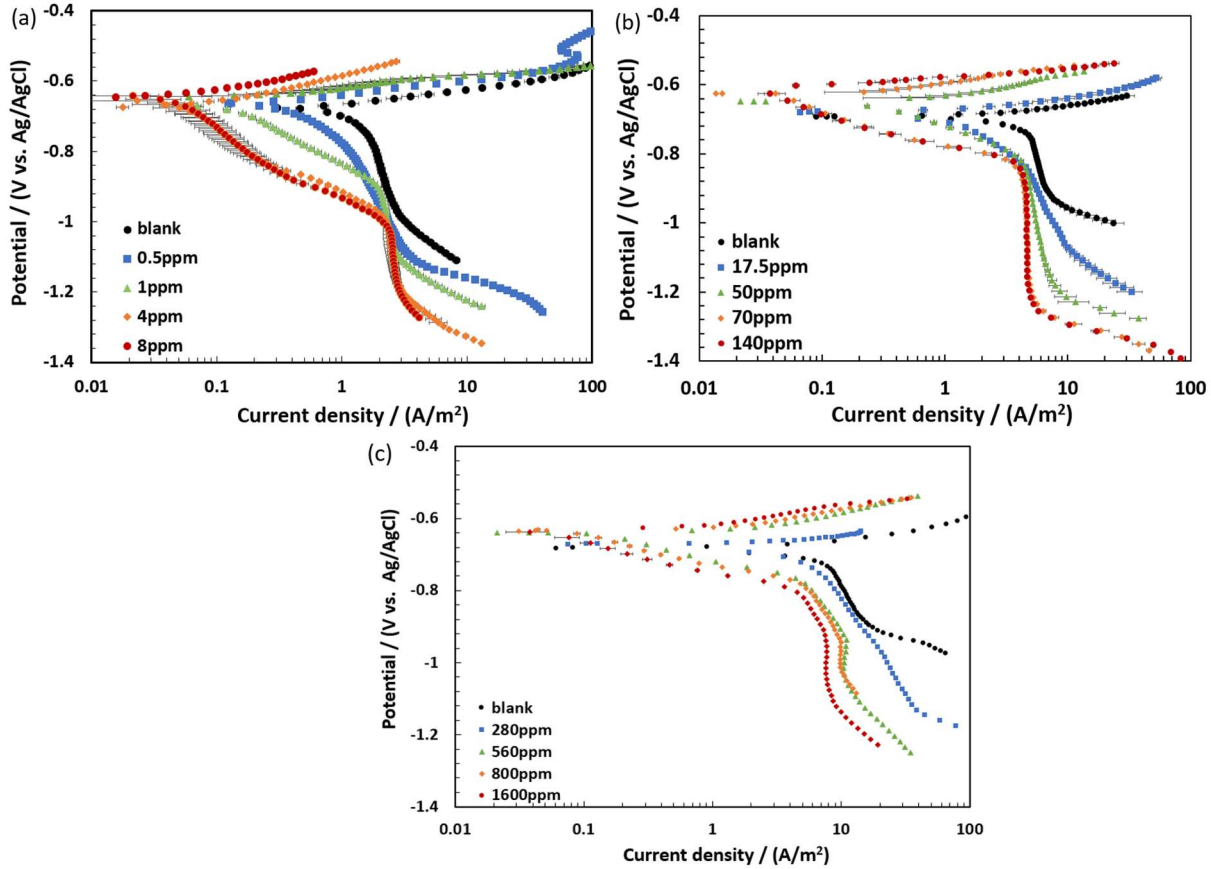


Figure 3. Sets of potentiodynamic polarization curves of C1018 in 5 wt.% NaCl with the addition of THP-C14 at different concentrations at (a) 25°C, (b) 55°C, and (c) 80°C.

At 80°C, Figure 3(c) shows that, when the concentration of corrosion inhibitor was decreased from 1600 ppm_w to 70 ppm_w, the potentiodynamic polarization curves became closer to the curves for the blank test, which was also consistent with the corrosion rate results. Besides, compared with the blank test, the addition of different concentrations of corrosion inhibitor seemed to retard both the anodic and cathodic reactions, which was due to the adsorption of organic corrosion inhibitors.^{9,17} Meanwhile, limiting currents were affected in inhibited cases at 1600 ppm, which is a noticeable deviation from what was observed at lower temperatures. Considering the inhibited corrosion rates are charge transfer controlled, the model developed by Domínguez, *et al.*^{9,17} is still applicable to the THP-C14 at 80°C with affected limiting current, on condition that the affected limiting current can be covered by updating the pre-existing model.

Temperature Effect on Inhibition Efficiency

The corrosion mitigation efficiency was calculated when the corrosion rate did not significantly change over time (less than ±0.01 mm/year between measurements). Equation (10) was used²⁴ to calculate the corrosion mitigation efficiency (ϵ):

$$\epsilon = 1 - \frac{(CR)_\theta}{CR} \quad (10)$$

Where $(CR)_\theta$ is the corrosion rate of the system with corrosion inhibitor and CR represents the corrosion rate of the same system without the inhibitor present. The inhibition performances at 25, 55 and 80°C were compared to understand the effect of temperature on inhibition behaviors of THP-C14. Table 2 summarizes the above results of the THP-C14 corrosion inhibitor model compound at 25, 55 and 80°C relating to the initial corrosion rate, the final corrosion rate and inhibition efficiency for different concentrations of CI at the three different temperatures. As the temperature increased, surface saturation concentration also increases. Moreover, the highest inhibition efficiency (95.3%) obtained at 25°C was noticeably lower than that at 55°C (98.3%) and 80°C (98.7%).

Table 2. Summary of the above results for the THP-C14 corrosion inhibitor model compound at 25, 55 and 80°C.

Temperature °C	Inhibitor concentration (ppm)	Initial corrosion rate (mm/year)	Final corrosion rate (mm/year)	Inhibition efficiency
25	4	2.0	0.11	94.5%
	8	1.9	0.09	95.3%
	16	1.8	0.09	95%
55	8.75	4.3	2.3	46.5%
	17.5	4.5	2.0	54.5%
	70	4.8	0.08	98.3%
80	8.75	5.9	7.3	-
	17.5	6.1	6.8	-
	560	6.0	0.3	95.0%
	800	6.0	0.18	97.0%
	1600	6.1	0.08	98.7%

Note: '-' suggests that the inhibition efficiency is not available, since inhibition were not observed experimentally.

Fitting of Different Adsorption Isotherms at 25, 55 and 80°C

In this section, five adsorption isotherm models are evaluated by fitting the steady state experimental data (C_{inh} vs θ_{eq}) by non-linearly regression method *via* Python scipy package brentq optimization function. The equilibrium fractional coverage (θ_{eq}) can be calculated based on the work of Hackerman, *et al.*,²⁰ using the following equation:

$$\theta_{eq} = \frac{(i_{corr})_{\theta=0} - (i_{corr})_{\theta}}{(i_{corr})_{\theta=0} - (i_{corr})_{\theta=max}} \quad (11)$$

where $(i_{corr})_{\theta=0}$ is the corrosion current without CI, $(i_{corr})_{\theta}$ is the corrosion current with CI, and $(i_{corr})_{\theta=max}$ is the steady-state corrosion current with CI at the metal surface saturation concentration with maximum surface coverage. Based on the methodology proposed above, corrosion currents and rates are interchangeable.

Python functions were used to minimize the sum of the difference between experimental data and calculated data by different isotherms. When the fitting was optimized, the Python code returned the optimized constant values and also the R^2 . From the coefficient of determination (R^2) of fitting, the

properness of these models to studied adsorption processes is discussed below. Figure 4 shows the fitting curves by different adsorption isotherm models at 25, 55 and 80°C. Table 3 lists the fitting results, including equilibrium constant (K_{AD}), fitting factor (R^2), as well as other constants. According to the fitting factor (R^2), the Langmuir model gave a good fit at both 25 and 55°C, which means the Langmuir model is good enough to be employed to describe the adsorption behaviors at these temperatures. For Temkin, the fitting result was poor mostly due to the lack of data points obtained at low inhibitor concentration. Frumkin, Flory-Huggins and Dhar-Flory-Huggins models can also give a good fit. More work is needed in understanding the physical meaning of the constants. When the temperature was increased to 80°C, the Langmuir model did not fit the experimental data very well. However, Frumkin, Flory-Huggins and Dhar-Flory-Huggins models displayed much better fitting performance than the Langmuir model. This difference could be related to the nature of the THP-C14 films formed on the RCE surface at 80°C. At 80°C, the THP-C14 film is multilayer, in which situation the Langmuir model may be no longer applicable. While it seems lower concentration experimental data are required to further evaluate these models. Also, there are still challenges in understanding the physical meanings of the constants in the different model equations. This work will be continued in the future.

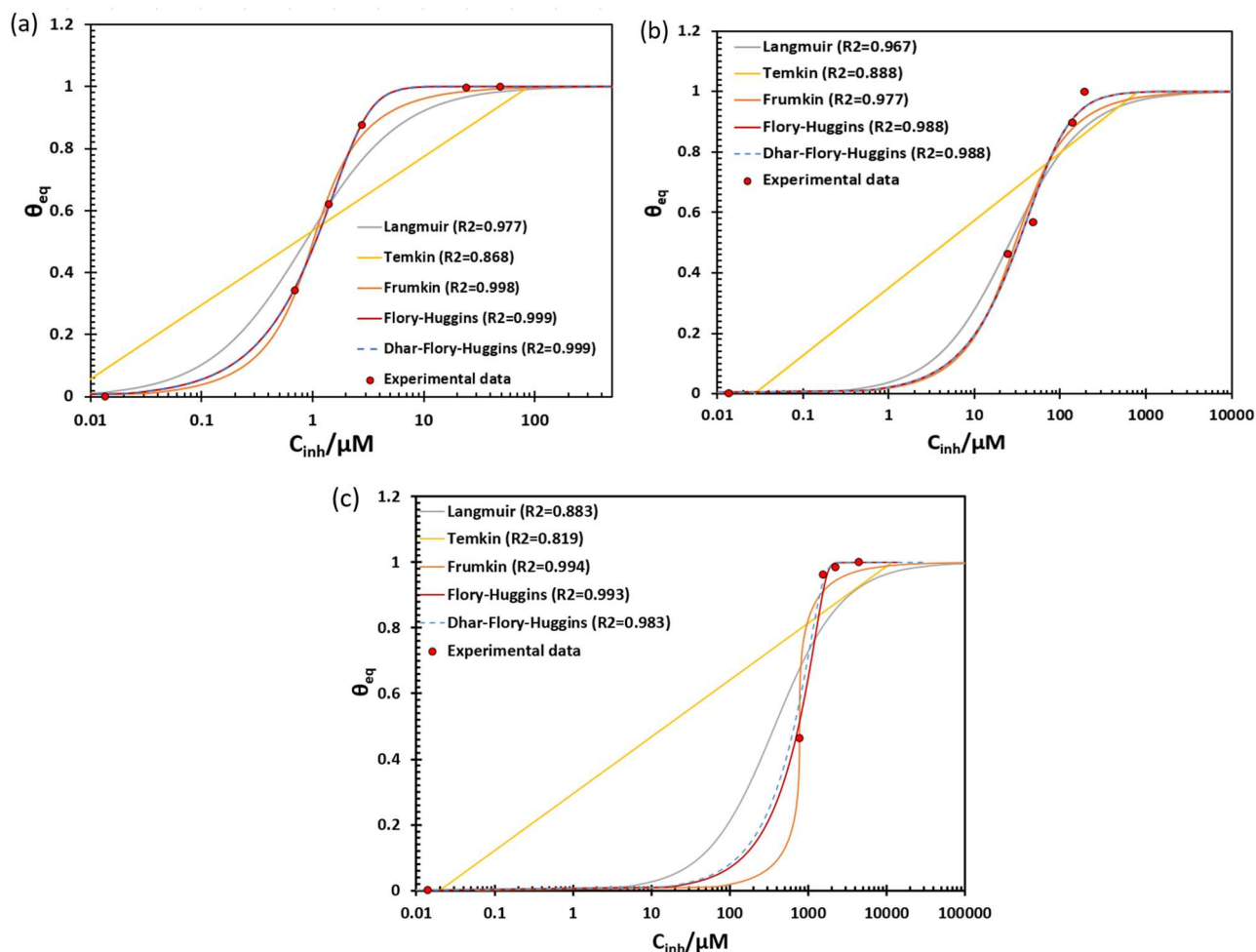


Figure 4. Different adsorption isotherm models (curves) fitting experimental data (red dots) with different THP-C14 concentrations at (a) 25°C (b) 55°C and (c) 80°C.

Table 3. Determination of the equilibrium constant, coefficient of determination (R^2), other constants by fitting experimental data with different adsorption models with different THP-C14 concentrations at 25, 55 and 80°C.

Temp. (°C)	Adsorption model	Equilibrium constant		Other parameters
		K_{AD} (L· μ mol ⁻¹)	R^2	
25	Langmuir	1.14	0.977	-
	Temkin	175	0.868	$g = 9.66$
	Frumkin	0.379	0.998	$f = 1.93$
	Flory-Huggins	2.06	0.999	$\delta = 0.279$
	Dhar-Flory-Huggins	1.18	0.999	$\delta = 0.279$
55	Langmuir	0.0386	0.967	-
	Temkin	36.4	0.888	$g = 10.3$
	Frumkin	0.0185	0.977	$f = 1.16$
	Flory-Huggins	0.0429	0.988	$\delta = 0.503$
	Dhar-Flory-Huggins	0.0354	0.988	$\delta = 0.503$
80	Langmuir	0.00266	0.883	-
	Temkin	50.1	0.819	$g = 13.3$
	Frumkin	0.000174	0.994	$f = 3.99$
	Flory-Huggins	0.00988	0.993	$\delta = 0.0699$
	Dhar-Flory-Huggins	0.00199	0.983	$\delta = 0.0999$

δ : number of solvent molecules substituted by one adsorbate molecule
 g : adsorbent-adsorbate interaction constant
 f : adsorbates interaction constant

From the above results, the Langmuir model can be chosen to describe the adsorption process at 25 and 55°C in the studied conditions. The Frumkin, Flory-Huggins and Dhar-Flory-Huggins models are preferred in describing the adsorption process at 80°C. The equilibrium constants of adsorption/desorption (K_{AD}) at 25, 55 and 80°C were determined by fitting the steady state experimental data. In order to obtain the other two constants, *i.e.*, adsorption and desorption constants (k_A and k_D), transient experimental data are required to be fitted by the transient form of the governing equation. However, only the Langmuir model, the simplest model, provides access to derive such information; for other models, it is difficult to obtain their transient form of the governing equations. In addition, since the transient experimental data can be affected by several factors, such as the volume of CI solvent and CI injection place, the accuracy of the determined adsorption and desorption constants by non-linear fitting with transient data needs to be considered. The steady state inhibition performance is more important than the transient process in inhibition evaluation.

Based on the above discussion, for future research, modeling the steady state inhibition behaviors, instead of the transient process, will be a key focus. The equilibrium constant (K_{AD}) will be the only adsorption constant that needs to be determined. This can help to simplify the testing protocol and accelerate the application of the developed inhibition model to commercial inhibitor packages.

Changes of Activation Energy at 25, 55 and 80°C

The potentiodynamic sweeps obtained for the blank and inhibited (at surface saturation concentration) conditions are analyzed to determine the change in activation energy due to the presence of the inhibitor.

The graphs for the 5 wt.% NaCl environment at 25, 55 and 80°C are plotted in Figure 5. Since experimental scatter can render this effort cumbersome, theoretical lines for the charge transfer components of the anodic and cathodic reactions are added to the graphs and fitted on the potentiodynamic sweeps. The theoretical lines are extracted from the mechanistic model for carbon dioxide corrosion of mild steel postulated by Nešić, *et al.*,²⁵ for both blank and inhibited conditions. Tafel slopes of 40 mV/dec for iron oxidation and 120 mV/dec for hydrogen ion reduction are adopted in the mechanistic model for fitting polarization curves. The current density ratio at the charge transfer part for both the anodic and cathodic reactions can then be more clearly determined, enabling the calculation of the change in activation energy, following the methodology presented earlier.

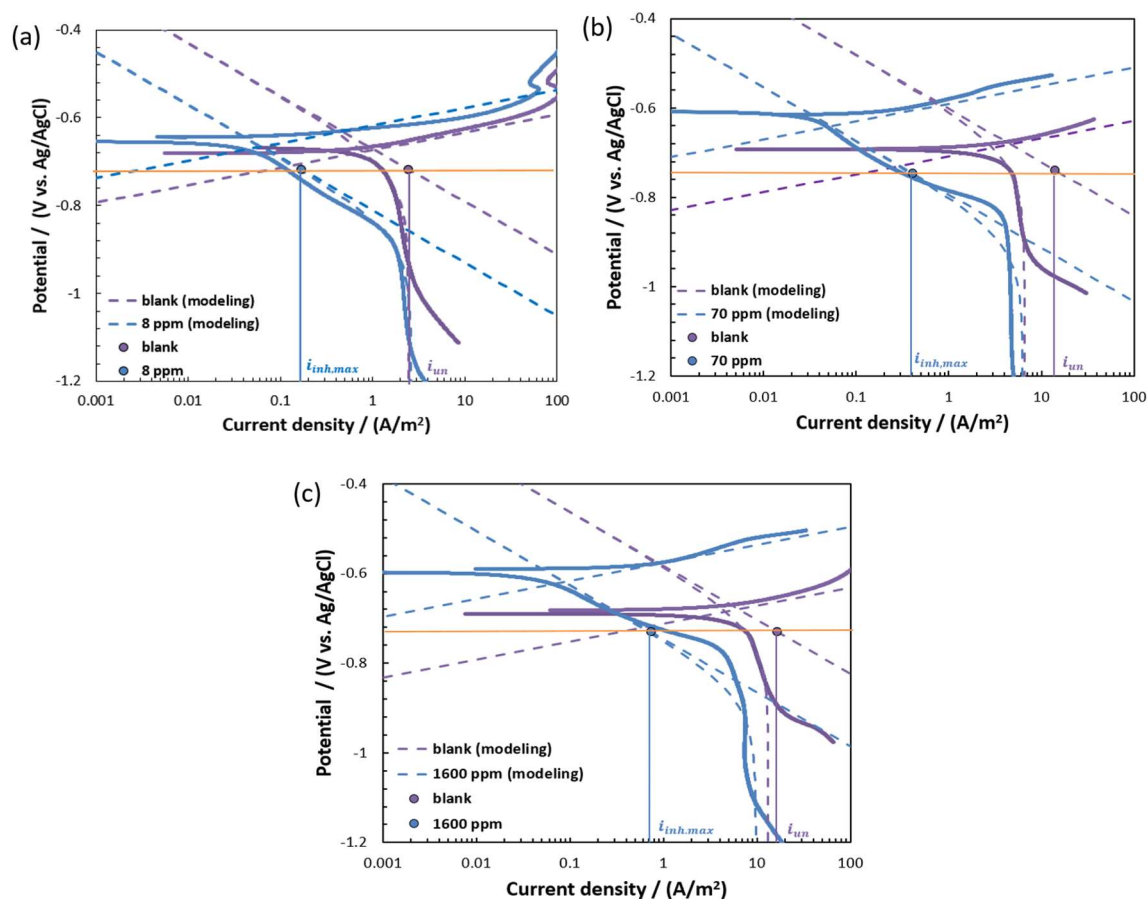


Figure 5. Illustration of current densities ratio ($i_{un}/i_{inh,max}$) determination at (a) 25°C (b) 55°C and (c) 80°C. The yellow line indicates at which potential the ratio of blank vs. inhibited current densities is taken.

For the blank tests, the theoretical lines for the anodic reaction (purple dashed line) overlap completely with measured curves. For the cathodic reaction, the effect of the limiting current needs to be taken into account, which is done readily by the mechanistic model. The cathodic charge transfer line was isolated from the total cathodic polarization curve considering mixing controlled corrosion by charge and mass transfer in blank condition. When the Cl concentration is above the surface saturation concentration, both anodic and cathodic charge transfer parts are fitted based on the measured curves *via* adjusting the exchange current density to mechanistically arbitrary, yet mathematically sound, value. Finally, the

charge transfer current densities of uninhibited and maximum inhibited (at surface saturation concentration) can be determined at any given potential. The activation energy difference is then calculated according to equation (9). Both anodic and cathodic parts are well fitted at both 25, 55 and 80°C, which implies that the chosen Tafel slopes are suitable and the mechanisms remain the same as the blank condition.

The change of activation energy can be obtained from uninhibited and inhibited current densities extracted from fitting graphs. The determined ($\Delta G_{inh,max}^{\#} - \Delta G_{un}^{\#}$) values at 25, 55 and 80°C are listed in Table 4. Comparing the values of activation energy changes, the inhibition effect on anodic and cathodic reactions are close to each other at 25°C. At higher temperatures, the anodic reaction seems to be retarded more than the cathodic reaction. The underlying reasons for this observation should be related to the effect of temperature on the inhibition behavior of THP-C14. More work is currently being undertaken to understand the observed phenomena.

Table 4. Summary of activation energy changes at 25, 55 and 80°C

Cl	Temperature	Reaction	$\Delta G_{inh,max}^{\#} - \Delta G_{un}^{\#}$ kJ/mol
THP-C14	25°C	Anodic	7.87
		Cathodic	6.74
	55°C	Anodic	19.7
		Cathodic	9.15
	80°C	Anodic	22.8
		Cathodic	9.16

CONCLUSIONS

The main conclusions of the present work are obtained under conditions for C1018 in 5 wt.% NaCl solution with pH 4.5 at 25, 55 and 80°C and 0.96 bar CO₂:

- The surface saturation concentrations of THP-C14 at 25, 55 and 80°C were determined to be between 1~4 ppm_w, 50~ 70 ppm_w and 800~1600 ppm_w, with corresponding inhibition efficiencies of 94.5%, 98.3% and 98.7%, respectively.
- At a constant inhibitor concentration, the inhibition efficiency/equilibrium coverage decreased with an increase in temperature. Failure cases of corrosion inhibition were observed at 80°C with low inhibitor concentrations for THP-C14 corrosion inhibitor. Higher concentrations of inhibitor were required to achieve ideal inhibition performance.
- THP-C14 retarded both anodic and cathodic reactions with no change in limiting current at 25°C and 55°C, which indicated that the inhibition model proposed by Dominguez, *et al.*^{9,17} should also be applicable to THP-C14 in the studied environment. At 80°C, limiting currents were affected in inhibited cases at 1600 ppm. Considering the inhibited CRs are charge transfer controlled, the model developed by Domínguez, *et al.*^{9,17} is still applicable to determine the corrosion efficiency of THP-C14 at 80°C, and the application of the model does not necessarily require that the limiting current remains the same for both inhibited and uninhibited cases.

- The Langmuir isotherm gives a reasonable fit for surface coverage at 25 and 55°C but not at 80°C. The reason behind this behavior change is still under investigation but must be related to differences in the characteristics of the CI film. For other models, it is difficult to obtain the transient form of the governing equations. Thus affect the “transitory” response of the inhibition only, *i.e.*, difficulty to have access to k_a and k_d .
- Changes in activation energies with and without inhibitors for both anodic and cathodic reactions at 55 and 80°C were higher than at 25°C.
- The change of activation energy of the anodic reaction was higher than for the cathodic reaction, except at 25°C where they were similar.

ACKNOWLEDGMENTS

This project has been supported by TOTAL transversal R&D project (MANA Project). The authors would like to thank TOTAL Energies for their financial support and valuable discussions.

REFERENCES

- [1] M. B. Kermani and D. Harrop, “The impact of corrosion on the oil and gas industry,” *SPE Prod. Facil.*, vol. 11, no. 3, pp. 186–190, 1996.
- [2] Y. Xiong, B. Brown, B. Kinsella, S. Nešić, and A. Pailleret, “Atomic force microscopy study of the adsorption of surfactant corrosion inhibitor films,” *Corrosion*, vol. 70, no. 3, pp. 247–260, 2014.
- [3] Y. Duda, R. Govea-Rueda, M. Galicia, H. I. Beltraén, and L. S. Zamudio-Rivera, “Corrosion inhibitors: Design, performance, and computer simulations,” *J. Phys. Chem. B*, vol. 109, no. 47, pp. 22674–22684, 2005.
- [4] V. Otieno-Alego, N. Huynh, T. Notoya, S. E. Bottle, and D. P. Schweinsberg, “Inhibitive effect of 4- and 5- carboxybenzotriazole on copper corrosion in acidic sulphate and hydrogen sulphide solutions,” *Corros. Sci.*, vol. 41, no. 4, pp. 685–697, 1999.
- [5] D. Chebabe, Z. Ait Chikh, N. Hajjaji, A. Srhiri, and F. Zucchi, “Corrosion inhibition of Armco iron in 1 M, HCl solution by alkyltriazoles,” *Corros. Sci.*, vol. 45, no. 2, pp. 309–320, 2003.
- [6] F. Bentiss, M. Lagrenee, M. Traisnel, and J. C. Hornez, “The corrosion inhibition of mild steel in acidic media by a new triazole derivative,” *Corros. Sci.*, vol. 41, no. 4, pp. 789–803, 1999.
- [7] Y. Ding, B. Brown, D. Young, and M. Singer, “Effectiveness of an imidazoline-type inhibitor against CO₂ corrosion of mild steel at elevated temperatures (120°C-150°C),” in *NACE - International Corrosion Conference Series*, 2018, no. 11622.
- [8] Z. Belarbi, T. N. Vu, F. Farel, D. Young, M. Singer, and S. Nešić, “Thiols as volatile corrosion inhibitors for top-of-the-line corrosion,” *Corrosion*, vol. 73, no. 7, pp. 892–899, 2017.
- [9] J. M. Domínguez Olivo, B. Brown, D. Young, and S. Nestic, “Electrochemical model of CO₂ corrosion in the presence of quaternary ammonium corrosion inhibitor model compounds,” in *NACE - International Corrosion Conference Series*, 2019, no. 13392.
- [10] N. Moradighadi, S. Lewis, J. M. Domínguez Olivo, D. Young, B. Brown, and S. Nestic, “Effect of

© 2022 Association for Materials Protection and Performance (AMPP). All rights reserved. No part of this publication may be reproduced, stored in a retrieval system, or transmitted, in any form or by any means (electronic, mechanical, photocopying, recording, or otherwise) without the prior written permission of AMPP.

Positions and opinions advanced in this work are those of the author(s) and not necessarily those of AMPP. Responsibility for the content of the work lies solely with the author(s).

alkyl tail length on CMC and mitigation efficiency using model quaternary ammonium corrosion inhibitors,” in *NACE - International Corrosion Conference Series*, 2019, no. 13004.

- [11] Y. Ding, “Mechanistic Understanding of CO₂ Corrosion Inhibition at Elevated Temperatures,” *PhD Thesis, Ohio Univ.*, 2019.
- [12] F. Bentiss, M. Lebrini, and M. Lagrenée, “Thermodynamic Characterization of Metal Dissolution and Inhibitor Adsorption Processes in Mild Steel/2,5-Bis(n-thienyl)- 1,3,4-Thiadiazoles/Hydrochloric Acid System,” *Corrosion Science*, vol. 47, no. 12, pp. 2915–2931, 2005.
- [13] K. Zhang, B. Xu, W. Yang, X. Yin, Y. Liu, and Y. Chen, “Halogen-substituted imidazoline derivatives as corrosion inhibitors for mild steel in hydrochloric acid solution,” *Corros. Sci.*, vol. 90, pp. 284–295, 2015.
- [14] K. Zhang, W. Yang, B. Xu, Y. Liu, X. Yin, and Y. Chen, “Corrosion inhibition of mild steel by bromide-substituted imidazoline in hydrochloric acid,” *J. Taiwan Inst. Chem. Eng.*, vol. 57, pp. 167–174, 2015.
- [15] C. Li, “Effect of corrosion inhibitor on water wetting and carbon dioxide corrosion in oil-water two-phase flow,” *Ph.D. Dissertation*. Ohio University, Athens, OH, 2009.
- [16] A. K. . Bockris, J O’M; Reddy, *Modern Electrochemistry - Volume 1*. 1999.
- [17] J. M. Domínguez Olivo, D. Young, B. Brown, and S. Nescic, “Effect of corrosion inhibitor alkyl tail length on the electrochemical process underlying CO₂ corrosion of mild steel,” in *NACE - International Corrosion Conference Series*, 2018, no. 11537.
- [18] Y. He, S. Ren, Z. Belarbi, X. Wang, D. Young, and M. Singer, “Micellization and Inhibition Efficiency,” in *in NACE - International Corrosion Conference Series*, 2021, no. 16872, pp. 1–16.
- [19] Z. Belarbi, F. Farelas, M. Singer, and S. Nescic, “Role of amine in the mitigation of CO₂ TOP of the line corrosion,” *Corrosion*, vol. 2, no. 7274, pp. 1256–1270, 2016.
- [20] T. Murakawa, S. Nagaura, and N. Hackerman, “Coverage of iron surface by organic compounds and anions in acid solutions,” *Corros. Sci.*, vol. 7, no. 2, pp. 79–89, 1967.
- [21] R. Gorte and L. D. Schmidt, “Desorption kinetics with precursor intermediates,” *Surf. Sci.*, vol. 76, no. 2, pp. 559–573, 1978.
- [22] L. T. Novak and D. C. Adriano, “Phosphorus Movement in Soils: Soil-Orthophosphate Reaction Kinetics,” *J. Environ. Qual.*, vol. 4, no. 2, pp. 261–266, 1975.
- [23] W. H. Kuan, S. L. Lo, C. M. Chang, and M. K. Wang, “A geometric approach to determine adsorption and desorption kinetic constants,” *Chemosphere*, vol. 41, no. 11, pp. 1741–1747, 2000.
- [24] S. Papavinasam, “Evaluation and Selection of Corrosion Inhibitors,” in *Uhlig’s Corrosion Handbook: Third Edition*, Hoboken, NJ, USA: John Wiley & Sons, Inc., 2011, pp. 1121–1127.
- [25] M. Nordsveen, S. Nešić, R. Nyborg, and A. Stangeland, “A mechanistic model for carbon dioxide corrosion of mild steel in the presence of protective iron carbonate films - Part 1: Theory and verification,” *Corrosion*, vol. 59, no. 5, pp. 443–456, 2003.